Flow Measurement and Instrumentation 52 (2016) 40–52

Contents lists available at ScienceDirect

Flow Measurement and Instrumentation

journal homepage: www.elsevier.com/locate/flowmeasinst

Coriolis flowmeter damping for two-phase flow due to decoupling

Nils T. Basse

Siemens A/S, Flow Instruments, Coriolisvej 1, 6400 Sønderborg, Denmark

ARTICLE INFO

Keywords:
Coriolis flowmeter
Damping theory
Two-phase flow
Decoupling

ABSTRACT

Coriolis flowmeters experience measurement errors due to both single- and two-phase flow. For two-phase flow, severe damping may occur, which leads to a (temporary) inability of the flowmeter to operate. The dominating part of the damping is caused by decoupling of the continuous and the dispersed phase. This paper presents the theory of damping due to decoupling in two-phase flow. Using a simple structural model, we provide examples of mixtures with water as the continuous phase. The dispersed phase is either air, or oil or sand.

1. Introduction

The "bubble theory" is the theory of Coriolis flowmeter operation in the case of entrained particles [1]. Entrained particles can cause (i) measurement errors and (ii) damping. We reviewed the bubble theory in [2] with emphasis on measurement errors. Equally important is the damping; in this paper, we study damping for the same mixtures discussed in [2]. The continuous phase (fluid) is water and the dispersed phase (particle) is either air, oil or sand.

Physically, what occurs during Coriolis flowmeter operation is that the motion of the fluid and the particles becomes decoupled. This causes damping and leads to the centre-of-mass no longer being on the axis of the vibrating tube(s). A broader overview of multi-phase flow in Coriolis flowmeters is provided in [3].

The paper is structured as follows: in Section 2 we present the theory of damping due to decoupling. A simple structural model for the tube is introduced in Section 3 followed by energy deliberations in Section 4. Quality factors are listed in Section 5. Combined expressions from the theory and the structural model are summarised in Section 6, while the results for the three mixtures can be found in Section 7. Application examples and measurements are discussed in Section 8, and we conclude in Section 9.

2. Damping due to decoupling

2.1. Mixture properties

The volume of the fluid–particle (f–p) mixture is:

$$V_{f-p} = V_p + V_f, \tag{1}$$

where V_p is the volume of the particles and V_f is the volume of the fluid. We can then write the volumetric particle fraction:

$$\alpha = \frac{V_p}{V_{f-p}} \tag{2}$$

The mixture density is:

$$\rho_{f-p} = \alpha\rho_p + (1-\alpha)\rho_f \tag{3}$$

We can then write the mixture mass as:

$$M_{f-p} = \rho_{f-p} V_{f-p} \tag{4}$$

The fluid mass is:

$$M_f = \rho_f V_f = \rho_f (1-\alpha) V_{f-p} \tag{5}$$

The particle mass is:

$$M_p = \rho_p V_p = \rho_p \alpha V_{f-p} \tag{6}$$

2.2. Theory

2.2.1. Container motion

We consider a rigid container oscillating at an angular frequency Ω with amplitude u in the z-direction. The fluid follows the container displacement u. We assume that the displacement is much smaller than the particle radius a: $u/a \ll 1$.

In complex notation, the container displacement is:

$$\begin{aligned} z_c &= u \times e^{i\Omega t} \\ Re(z_c) &= u \times \cos(\Omega t) \\ Im(z_c) &= u \times \sin(\Omega t) \end{aligned} \tag{7}$$

By differentiating, the container velocity is:

E-mail address: nils.basse@npb.dk.

http://dx.doi.org/10.1016/j.flowmeasinst.2016.09.005
Received 4 May 2016; Received in revised form 21 September 2016; Accepted 22 September 2016
Available online 27 September 2016
0955-5986/ © 2016 Elsevier Ltd. All rights reserved.

$$v_c = i\Omega u \times e^{i\Omega t}$$
$$Re(v_c) = -\Omega u \times \sin(\Omega t)$$
$$Im(v_c) = \Omega u \times \cos(\Omega t) \quad (8)$$

Finally, the container acceleration is:

$$a_c = -\Omega^2 u \times e^{i\Omega t}$$
$$Re(a_c) = -\Omega^2 u \times \cos(\Omega t)$$
$$Im(a_c) = -\Omega^2 u \times \sin(\Omega t) \quad (9)$$

2.2.2. Force on particles

The force on the particles from the container is:

$$F_p = -F_{f,z} = -(\rho_f - \rho_p) V_p a_c F, \quad (10)$$

see Eq. (65) in [2]. Here, F is the reaction force coefficient defined in Eq. (66) in [2]. F depends on the Stokes number and the particle-to-fluid density and dynamic viscosity ratios.

Expanding the complex terms we have:

$$F_p = -(\rho_f - \rho_p) V_p \times [(Re(a_c) + iIm(a_c)) \times (Re(F) + iIm(F))]$$
$$Re(F_p) = -(\rho_f - \rho_p) V_p \times [Re(a_c)Re(F) - Im(a_c)Im(F)]$$
$$Im(F_p) = -(\rho_f - \rho_p) V_p \times [Im(a_c)Re(F) + Re(a_c)Im(F)] \quad (11)$$

2.2.3. Work done per cycle on particles

The work done per cycle on the particles by the container is:

$$W_p = \int_0^{2\pi/\Omega} Re(F_p) \times Re(v_c) \mathrm{d}t \quad (12)$$

To proceed, we need the real part of the force on the particles:

$$Re(F_p) = (\rho_f - \rho_p) V_p \Omega^2 u \times [\cos(\Omega t) Re(F) - \sin(\Omega t) Im(F)] \quad (13)$$

The integrand in Eq. (12) is a combination of Eqs. (8) and (13). The $\cos(\Omega t)\sin(\Omega t)$ term is zero when integrating over a cycle, so we get:

$$W_p = (\rho_f - \rho_p) V_p \Omega^3 u^2 Im(F) \times \int_0^{2\pi/\Omega} \sin^2(\Omega t) \mathrm{d}t = (\rho_f - \rho_p) V_p \Omega^3 u^2 Im(F) \times \frac{\pi}{\Omega} = \pi (\rho_f - \rho_p) V_p \Omega^2 u^2 Im(F) \quad (14)$$

Using Eq. (2), we can rewrite this as:

$$W_p = \pi (\rho_f - \rho_p) \alpha V_{f-p} \Omega^2 u^2 Im(F) \quad (15)$$

This work leads to the decoupled motion of particles and fluid. The drag between the fluid and the particles leads to a higher mixture temperature. Simple estimates for the mixture examples we consider show that this temperature increase is negligible, see Appendix A.

We observe that work scales:

- with the fluid–particle density difference;
- linearly with $\alpha V_{f-p} = V_p$ and $Im(F)$ and
- quadratically with Ω and u.

2.2.4. Power dissipated per cycle on particles

The power dissipated per cycle on the particles by the container is:

$$P_p = \frac{\Omega}{2\pi} W_p = \frac{1}{2} (\rho_f - \rho_p) \alpha V_{f-p} \Omega^3 u^2 Im(F) \quad (16)$$

Power dissipation modelling has been discussed in Chapter 7 of [4]: given Ω and u, the particle motion equations were solved to yield the deflection of the particles and the particle–fluid phase shift.

Instead of this approach, we obtain the corresponding information from $Im(F)$ which can be calculated analytically.

3. Tube structural mechanics

We now introduce a simple mechanical model of a tube that is used instead of the rigid container. The tube is fixed at both ends with a force applied at the midpoint. This means that u becomes a function of (i) the applied midpoint force and (ii) the position along the tube x.

3.1. Static deflection

We proceed according to [5]. Initially, we assume that the tube is surrounded by vacuum, both inside and outside.

The applied midpoint force is P, the length of the tube is L, the modulus of elasticity of the tube is E and the moment of inertia is I.

The deflection curve is:

$$u = -\frac{Px^2}{48EI}(3L - 4x) \quad (0 \le x \le L/2) \quad (17)$$

The maximum deflection at the midpoint is:

$$u_{\max} = -u(x = L/2) = \frac{PL^3}{192EI} \quad (18)$$

The mean deflection is:

$$\overline{u} = -\frac{\int_0^L u(x)\mathrm{d}x}{L} = \frac{P}{48EI}\left(\frac{L}{2}\right)^3 = \frac{PL^3}{384EI} = \frac{u_{\max}}{2} \quad (19)$$

The mean deflection squared is:

$$\overline{u^2} = \frac{\int_0^L u(x)^2\mathrm{d}x}{L} = \frac{13}{560} \times \frac{P^2L^6}{48^2E^2I^2} = \frac{13}{35} \times u_{\max}^2 \quad (20)$$

In the following, we replace the deflection squared with the mean deflection squared:

$$u^2 \to \overline{u^2} \quad (21)$$

The inner tube diameter is d_i and the outer tube diameter is d_o.

The tube moment of inertia is:

$$I_{\text{tube}} = \frac{\pi (d_o^4 - d_i^4)}{64} \quad (22)$$

With tube density ρ_{tube} we can write the tube mass:

$$M_{\text{tube}} = \rho_{\text{tube}} V_{\text{tube}} = \rho_{\text{tube}} L\pi \left[\left(\frac{d_o}{2}\right)^2 - \left(\frac{d_i}{2}\right)^2\right] = \rho_{\text{tube}} LA, \quad (23)$$

where A is the tube cross-sectional area.

3.1.1. Steel tube example

We consider a steel tube at room temperature:

- E=200 GPa.
- ρ_{tube} = 7850 kg/m^3.
- L=0.25 m.
- d_i = 20 mm.
- d_o = 22 mm.
- P=1 mN.

The moment of inertia is:

$$I_{\text{steel tube}} = 3.6e - 9 \text{ m}^4 \quad (24)$$

The deflection at the midpoint as a function of P is:

$$u_{\max,\text{steel tube}} = P \times 1.1e - 7 \text{ m} \quad (25)$$

This means that for P=1 mN, the midpoint deflection is 0.1 nm.

The deflection curve is shown in Fig. 1.

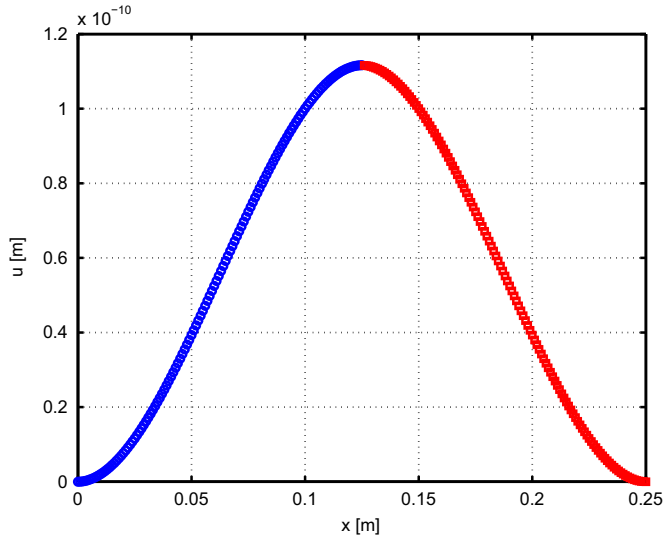

Fig. 1. Static deflection curve for steel tube example.

3.2. Vibration

Vibration modes are found as described in [6]. The frequency of mode number i is:

$$f_i = \frac{\omega_i}{2\pi} = \frac{1}{2\pi}\frac{T_i^2}{L^2}\sqrt{\frac{EI}{\rho_{\text{tube}}A}}, \tag{26}$$

where T_i are roots of a frequency equation defined in [6]. For the fundamental mode (i=1), $T_1 = 4.730$.

The frequency of the fundamental mode is: $f_1 = 2138$ Hz. The mode shapes for the first five modes are shown in Fig. 2.

The tube spring constant (force/deflection) is:

$$k_{\text{tube}} = \frac{P}{u_{\max}} = \frac{192EI}{L^3} \tag{27}$$

The angular frequency of the fundamental mode can also be written as:

$$\omega_1 = \sqrt{\frac{k_{\text{tube}}}{M^*_{\text{tube}}}}, \tag{28}$$

where M^*_{tube} is the effective mass of the tube.

Combining Eqs. (26) and (28) the effective tube mass can be written as:

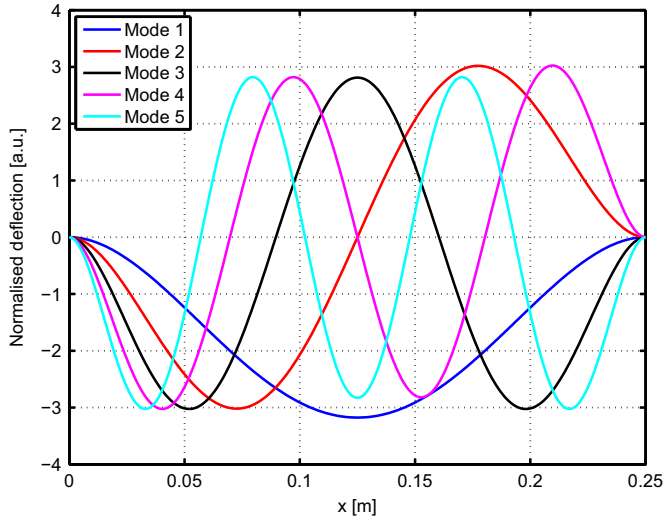

Fig. 2. Mode shapes of the first five modes for steel tube example.

$$M^*_{\text{tube}} = \frac{192}{T_1^4} \times M_{\text{tube}} \tag{29}$$

We can include a mixture by defining the total effective mass which is the sum of the effective tube mass and the effective mixture mass:

$$M^*_{\text{total}} = \frac{192}{T_1^4} \times (M_{\text{tube}} + V_{f-p}\rho_a) \tag{30}$$

In Eq. (30) we use the apparent density ρ_a [2] instead of the mixture density:

$$\rho_a = \rho_f\left[1 - \alpha Re(F)\left(\frac{\rho_f - \rho_p}{\rho_f}\right)\right] \tag{31}$$

Including the mixture, the fundamental angular frequency is:

$$\omega_{f-p} = \omega_1 = \sqrt{\frac{k_{\text{tube}}}{M^*_{\text{total}}}} \tag{32}$$

Eqs. (30) and (32) are coupled through the apparent density defined in Eq. (31): $Re(F)$ is frequency-dependent. Examples of the fundamental frequency are presented in Section 7.1. We refer to [7,8] for more details on Coriolis flowmeter mode frequencies.

3.3. Forced response

We proceed according to [6].

For a forced response, the static deflection u of the modes is amplified by a magnification factor to obtain the dynamic deflection. The magnification factor is:

$$\beta_i = \frac{1}{\sqrt{\left(1 - \frac{\Omega^2}{\omega_i^2}\right) + \left(\frac{2\gamma_i\Omega}{\omega_i}\right)^2}}, \tag{33}$$

where $\gamma_i = \frac{\Omega}{2\omega_i Q}$ is the damping ratio and Q is the quality factor, see Section 5.

Initially, we consider an undamped system ($\gamma = 0$) where the angular forcing frequency Ω is different from the angular mode frequencies ω_i.

As examples we treat 100 Hz and 2000 Hz forcing frequencies without a fluid inside. We consider the steady-state forced response and disregard the transient free response. The magnification factors are:

- $\beta_1(\Omega/2\pi = 100[\text{Hz}]) = 1.00$.
- $\beta_1(\Omega/2\pi = 2000[\text{Hz}]) = 8.03$.

The deflection for 100 Hz is almost the same as in Fig. 1, see the left-hand plot in Fig. 3.

From Fig. 3 we also note that the deflection of modes 2–5 is small compared to mode 1. In the remainder of this paper, we only treat the fundamental mode.

4. Energy considerations

4.1. Tube energy

From Eq. (8) we find that the maximum tube (container) velocity is:

$$v_{c,\max} = \max(Re(v_c)) = \Omega u \tag{34}$$

The total tube energy is:

$$E_{\text{tube}} = \frac{M_{\text{tube}}}{2L}\int_0^L v_{c,\max}^2\,\mathrm{d}x = \frac{1}{2}M_{\text{tube}}\Omega^2 \times \frac{\int_0^L u(x)^2\mathrm{d}x}{L} = \frac{1}{2}M_{\text{tube}}\Omega^2 \times \overline{u^2}$$
$$= \frac{1}{2}M_{\text{tube}}\Omega^2 \times \left[\frac{13}{560} \times \frac{P^2L^6}{48^2E^2I^2}\right] \tag{35}$$

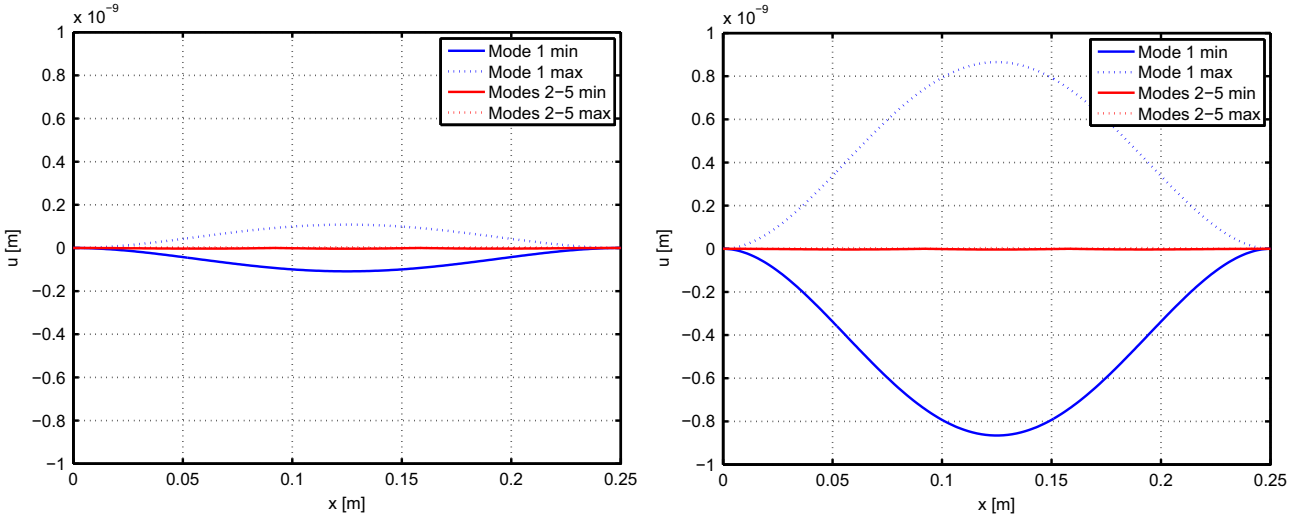

Fig. 3. Deflection curves for steel tube example. Left: $\Omega/2\pi = 100$ Hz and right: $\Omega/2\pi = 2000$ Hz.

4.2. Fluid energy

The fluid is assumed to move with the tube, so the fluid energy can be found simply by replacing M_{tube} with M_f in Eq. (35):

$$E_f = \tfrac{1}{2} M_f \Omega^2 \times \overline{u^2} \tag{36}$$

4.3. Particle energy

The particle motion is decoupled from the common motion of the tube and the fluid. The particle velocity is derived in [1] to be:

$$v_p = v_c F \tag{37}$$

Using Eq. (8) we can write the real part of the particle velocity:

$$\begin{aligned} Re(v_p) &= -\Omega u\left[\sin(\Omega t) Re(F) + \cos(\Omega t) Im(F)\right] = -\Omega u \sqrt{Re(F)^2 + Im(F)^2} \\ &\cos\left(\Omega t - \arctan\left(\frac{Re(F)}{Im(F)}\right)\right) = -\Omega u \sqrt{Re(F)^2 + Im(F)^2} \\ &\sin\left(\Omega t + \pi/2 - \arctan\left(\frac{Re(F)}{Im(F)}\right)\right) = -\Omega u \times B \sin(\Omega t + \phi), \end{aligned} \tag{38}$$

where

$$B = \sqrt{Re(F)^2 + Im(F)^2} \tag{39}$$

is the decoupling ratio [4] and

$$\phi = \pi/2 - \arctan\left(\frac{Re(F)}{Im(F)}\right) \tag{40}$$

is the phase shift.

The real part of the particle velocity has a maximum of:

$$v_{p,\max} = \max(Re(v_p)) = \Omega u \times B \tag{41}$$

Therefore the total particle energy is:

$$E_p = \frac{M_p}{2L} \int_0^L v_{p,\max}^2 \, \mathrm{d}x = \frac{1}{2} M_p \Omega^2 \times \frac{\int_0^L u(x)^2 \mathrm{d}x}{L} \times B^2 = \frac{1}{2} M_p \Omega^2 \times \overline{u^2} \times B^2 \tag{42}$$

4.4. Total energy

The total energy is the sum of the tube, fluid and particle energy:

$$E_{\text{total}} = \frac{1}{2}\Omega^2 \times \overline{u^2} \times [M_{\text{tube}} + M_f + M_p \times B^2] = \frac{1}{2}\Omega^2 \times \overline{u^2} \times M_{\text{eff}} \tag{43}$$

5. Quality factor

The quality factor Q is defined as:

$$Q = 2\pi \frac{E_{\text{total}}}{W}, \tag{44}$$

where E_{total} is defined in Eq. (43).

5.1. Structural damping

According to [6], we model structural damping as an equivalent viscous damping. The work dissipated per cycle by the damping force is:

$$W_{\text{tube}} = \pi c \Omega \overline{u^2}, \tag{45}$$

where c is the damping constant.

The quality factor of the tube is:

$$Q_{\text{tube}} = 2\pi \frac{E_{\text{total}}}{W_{\text{tube}}} = 2\pi \frac{\frac{1}{2} M_{\text{eff}} \Omega^2}{\pi c \Omega} = \frac{M_{\text{eff}} \Omega}{c} \tag{46}$$

The power dissipated per cycle by the damping force is:

$$P_{\text{tube}} = \frac{\Omega}{2\pi} W_{\text{tube}} = \Omega \frac{E_{\text{total}}}{Q_{\text{tube}}} \tag{47}$$

5.1.1. Steel tube example

To find the damping constant c for our case, we assume that (i) $Q_{\text{tube}} = 10^4$ for pure water and (ii) c is independent of the mixture properties:

$$c = \frac{M_{\text{eff}} \Omega}{Q_{\text{tube}}} = \frac{(M_{\text{tube}} + M_f)\Omega}{Q_{\text{tube}}} \tag{48}$$

Inserting numbers for pure water and using $\Omega = \omega_{f-p}$ we arrive at:

$$c = \frac{(0.1295\ \text{kg} + 0.0784\ \text{kg}) \times 1.06 \times 10^4\ \text{s}^{-1}}{10^4} = 0.22\ \text{kg/s} \tag{49}$$

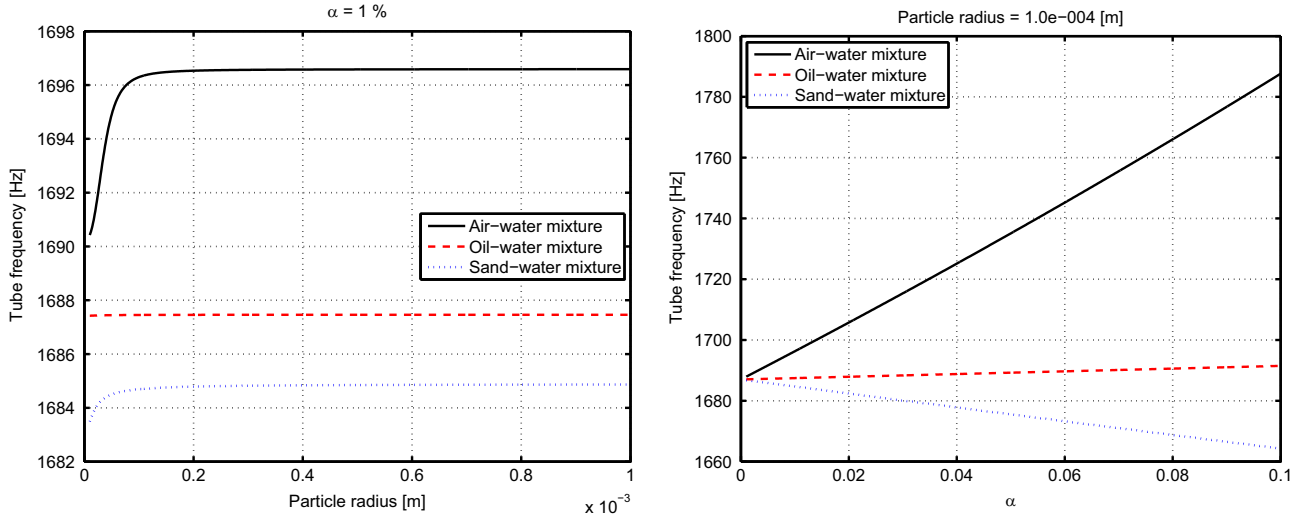

Fig. 4. Driver frequency for mixtures. Left: fixed α and right: fixed particle radius.

5.2. Damping due to decoupling

Using W_p from Eq. (15), we find that the quality factor due to decoupling is:

$$Q_p = 2\pi\frac{E_{\text{total}}}{W_p} = 2\pi\frac{\frac{1}{2}M_{\text{eff}}\Omega^2}{\pi(\rho_f-\rho_p)\alpha V_{f-p}\Omega^2 Im(F)} = \frac{M_{\text{eff}}}{(\rho_f-\rho_p)\alpha V_{f-p}Im(F)} \tag{50}$$

5.3. Total damping

Assuming that the only damping in our system is structural damping and damping due to decoupling, the total work per cycle is given by:

$$W_{\text{total}} = W_{\text{tube}} + W_p = \overline{u^2}\times(\pi c\Omega + \pi(\rho_f-\rho_p)\alpha V_{f-p}\Omega^2 Im(F)) \tag{51}$$

The corresponding total quality factor is:

$$Q_{\text{total}} = 2\pi\frac{E_{\text{total}}}{W_{\text{total}}} = \frac{M_{\text{eff}}\Omega^2}{c\Omega+(\rho_f-\rho_p)\alpha V_{f-p}\Omega^2 Im(F)} = \frac{M_{\text{eff}}}{\frac{c}{\Omega}+(\rho_f-\rho_p)\alpha V_{f-p}Im(F)} \tag{52}$$

Note that $\frac{c}{\Omega}$ in the denominator of Eq. (52) can also be expressed as $\frac{M_{\text{eff}}}{Q_{\text{tube}}}$, see Eq. (46).

6. Combined expressions

The driver angular frequency is set equal to the fundamental angular frequency from Eq. (32):

$$\Omega = \omega_{f-p} \tag{53}$$

Using this assumption, Eq. (33) yields:

$$\beta_1(\Omega=\omega_1=\omega_{f-p}) = Q_{\text{total}} \tag{54}$$

We modify Eq. (20) to include Q_{total}:

$$\overline{u^2} \to \overline{u^2}\times Q_{\text{total}}^2 = \frac{13}{560}\times\frac{P^2L^6}{48^2E^2I^2}\times Q_{\text{total}}^2 \tag{55}$$

Using Eqs. (15), (16) and (43), we can derive the full expressions for the work and the dissipated power per cycle and the total energy as follows:

$$W_p = \pi(\rho_f-\rho_p)\alpha V_{f-p}\Omega^2 Im(F)\overline{u^2} = \pi(\rho_f-\rho_p)\alpha V_{f-p}\Omega^2 Im(F)\times\frac{13}{560}\times\frac{P^2L^6}{48^2E^2I^2}\times Q_{\text{total}}^2 \tag{56}$$

$$P_p = \frac{1}{2}(\rho_f-\rho_p)\alpha V_{f-p}\Omega^3 Im(F)\overline{u^2} = \frac{1}{2}(\rho_f-\rho_p)\alpha V_{f-p}\Omega^3 Im(F)\times\frac{13}{560}\times\frac{P^2L^6}{48^2E^2I^2}\times Q_{\text{total}}^2 \tag{57}$$

$$E_{\text{total}} = \frac{1}{2}M_{\text{eff}}\Omega^2\times\frac{13}{560}\times\frac{P^2L^6}{48^2E^2I^2}\times Q_{\text{total}}^2 \tag{58}$$

7. Results

In this section, we analyse our particle examples of air, sand and oil. For all cases, the fluid is water.

In Section 7.1, we compare the three mixtures and in Section 7.2, we treat the individual mixtures.

The reaction force coefficient F depends on the particle size through the Stokes number:

$$Stk = a\sqrt{\frac{\omega_{f-p}\rho_f}{2\mu_f}} = a\sqrt{\frac{\omega_{f-p}}{2\nu_f}}, \tag{59}$$

where ν_f is the kinematic viscosity, which is 1.004×10^{-6} m^2/s for water at room temperature. For water with 1% air, the maximum $Im(F) = 0.81$ is found for Stk=2.6, see Fig. 5. Stk only varies slightly with α, see the left-hand plot in Fig. 9.

7.1. Comparison of mixtures

For the comparison of mixtures, we analyse two cases: (i) fixed α and changing particle radii and (ii) fixed particle radius and changing α. Corresponding driver frequencies are shown in Fig. 4. When α changes to 10% then the frequency changes by up to about 6%.

7.1.1. Fixed α, changing particle radius

In this section, α = 1%, and the particle radii vary from 10 μm to 1 mm.

Stk and $Im(F)$ are shown in Fig. 5. Stk increases linearly with particle radius. $Im(F)$ has a maximum (minimum) below 50 μm; however, the exact peak/trough particle radius changes depending on the particular mixture.

The Q (Q_{total} from Eq. (52)) is shown in Fig. 6. The lowest Q

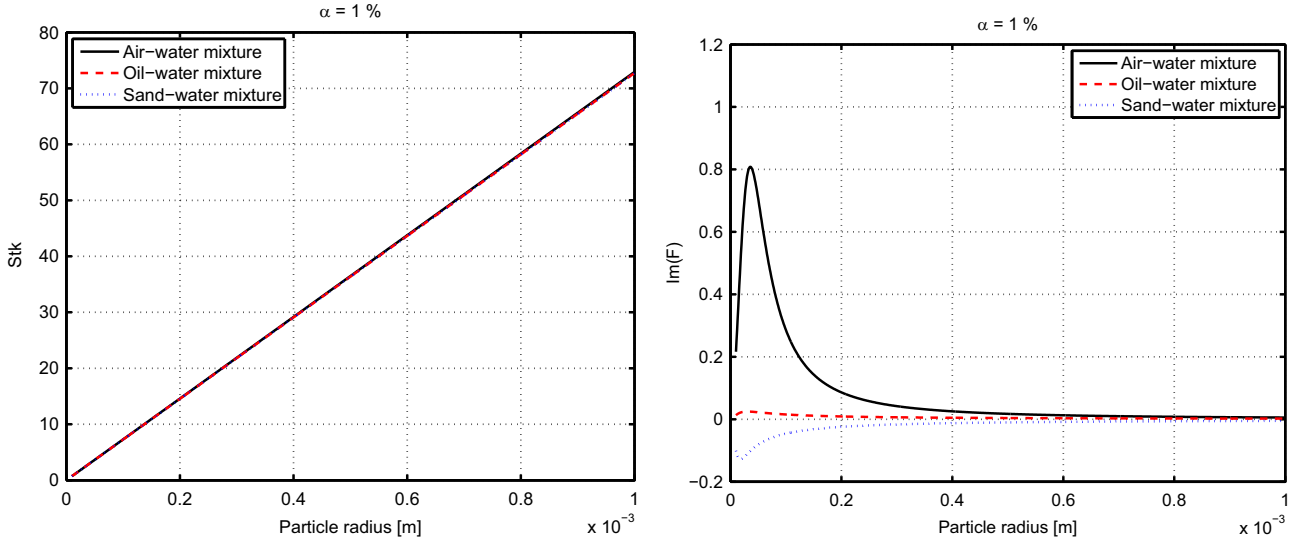

Fig. 5. Fixed α. Left: *Stk* vs. particle radius and right: *Im*(*F*) vs. particle radius.

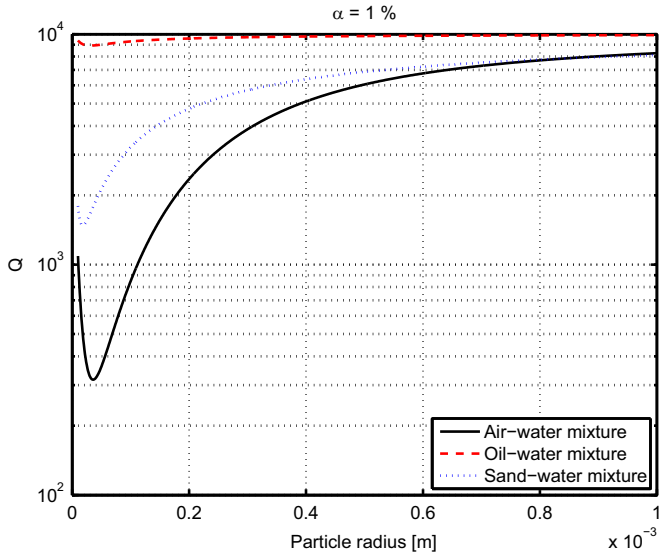

Fig. 6. Fixed α. Q vs. particle radius.

observed for the air–water mixture is about 300. For the sand–water mixture the minimum Q is 1500. Q does not significantly decrease for the oil–water mixture.

The work and power per cycle are shown in Fig. 7. Maximum work is found for different particle radii for the mixtures and is of the order 10^{-9} J. The corresponding power maxima are at about 10^{-6} W.

The mean deflection of the tube and the total energy are shown in Fig. 8. The damping – especially for air and sand – leads to a significant decrease of the deflection for our fixed driver force. This is reflected in the low total energy.

7.1.2. Fixed particle radius, changing α

In this section, the particle radius $a = 0.1$ mm and α varies from 0.1% to 10%.

Stk and *Im*(*F*) are shown in Fig. 9. *Stk* is almost constant since it only changes with the square root of the driver frequency. *Im*(*F*) is also almost constant.

Q is shown in Fig. 10. The lowest Q is observed for the air–water mixture. Where damping due to decoupling dominates over structural damping, Q is inversely proportional to α.

The work and power per cycle are shown in Fig. 11. Maximum work is found for different particle radii for the mixtures and is of the order 10^{-9} J. The corresponding power maxima are at about 10^{-6} W.

The mean deflection of the tube and the total energy are shown in Fig. 12. The damping – especially for air and sand – leads to a significant decrease of the deflection for our fixed driver force. This is reflected in the low total energy.

7.2. Individual mixtures

In this section we present results for the individual mixtures. This is to obtain the complete overview of the behaviour over the range of α and the particle sizes being considered.

7.2.1. Air–water mixture

The work per cycle for the air–water mixture is shown in Fig. 13. The work is the highest for large particle radii.

The natural logarithm of Q is shown in Fig. 14. We use the natural logarithm to make the plot clearer. The minimum Q is found for particle radii below 0.1 mm, independent of α.

7.2.2. Oil–water mixture

The work per cycle for the oil–water mixture is shown in Fig. 15. The work is the highest for small particle radii.

The natural logarithm of Q is shown in Fig. 16. The minimum Q is found for particle radii below 0.1 mm, independent of α.

7.2.3. Sand–water mixture

The work per cycle for the sand–water mixture is shown in Fig. 17. The work is the highest for large particle radii.

The natural logarithm of Q is shown in Fig. 18. The minimum Q is found for particle radii below 0.1 mm, independent of α.

8. Discussion

8.1. Driver force design guide

In this paper we have used a fixed force P. This leads to a changing tube deflection for different Q_{total}. To make this clear, we modify Eq. (19) to include Q_{total}:

$$\bar{u} \rightarrow \bar{u} \times Q_{\text{total}} = \frac{PL^3}{384EI} \times Q_{\text{total}} \tag{60}$$

Vice versa, if we want to have a fixed mean deflection, then the force P changes. For example, if we require a fixed deflection amplitude $\overline{u_{\text{fixed}}} = 0.5$ μm, then the force needed is:

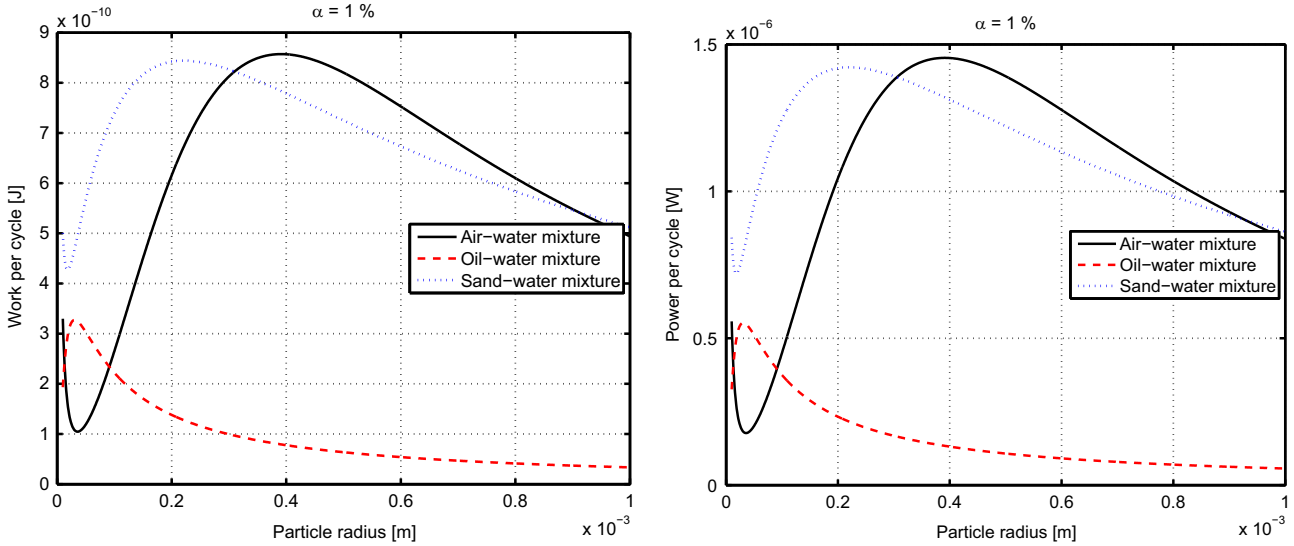

Fig. 7. Fixed α. Left: W_P vs. particle radius and right: P_P vs. particle radius.

$$P_{\text{dynamic}} = \overline{u}_{\text{fixed}} \times \frac{384EI}{L^3 \times Q_{\text{total}}} \tag{61}$$

We show the force required for the cases of fixed α and fixed particle radius in Fig. 19. For the air–water mixture, the maximum force needed is 0.1 N.

To obtain a complete overview of the force required for an air–water mixture, a contour plot is shown in Fig. 20. A maximum force of 0.28 N is found for 10% air with a particle size of around 40 μm.

8.2. Thermal effects

Our analytical expressions allow estimates to be made for temperatures other than room temperature.

As an example, we assume that the temperature of an air–water mixture and the tube is 80 °C (high temperature) instead of room temperature. The tube is allowed to expand freely in the longitudinal direction.

The steel tube material data is modified from the values in Section 3.1.1 to:

- E=195 GPa.
- $\rho_{\text{tube}} = 7820\ \text{kg/m}^3$.

The original material parameters used for air and water at room temperature can be found in Table 2 in [2]. These are modified to the values in Table 1.

The natural logarithm of Q is shown in Fig. 21. The left-hand plot is for damping at room temperature and the right-hand plot is for damping at the high temperature. Q is somewhat higher for the high temperature case. As a consequence, we can state that the high temperature damping is somewhat lower than the room temperature damping.

8.3. Comparison to measurements

Presenting the theory of damping due to two-phase flow, it is very interesting to compare the results to measurements. We have not found two-phase damping measurements for Coriolis flowmeters; however, measurements to study two-phase flow damping in steam generators are available [9]. Below, we make a qualitative comparison between these measurements and the bubble theory.

The measurements were made using air–water mixtures. Here, the volumetric particle fraction α is also known as the gas-void fraction

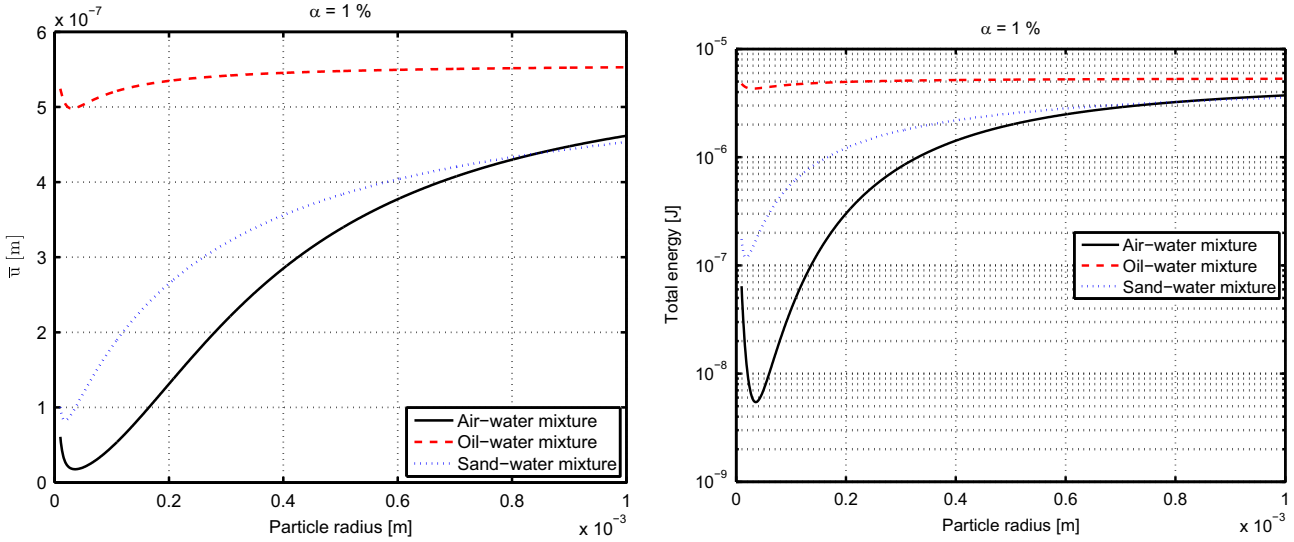

Fig. 8. Fixed α. Left: $\bar{u}$ vs. particle radius and right: E_{total} vs. particle radius.

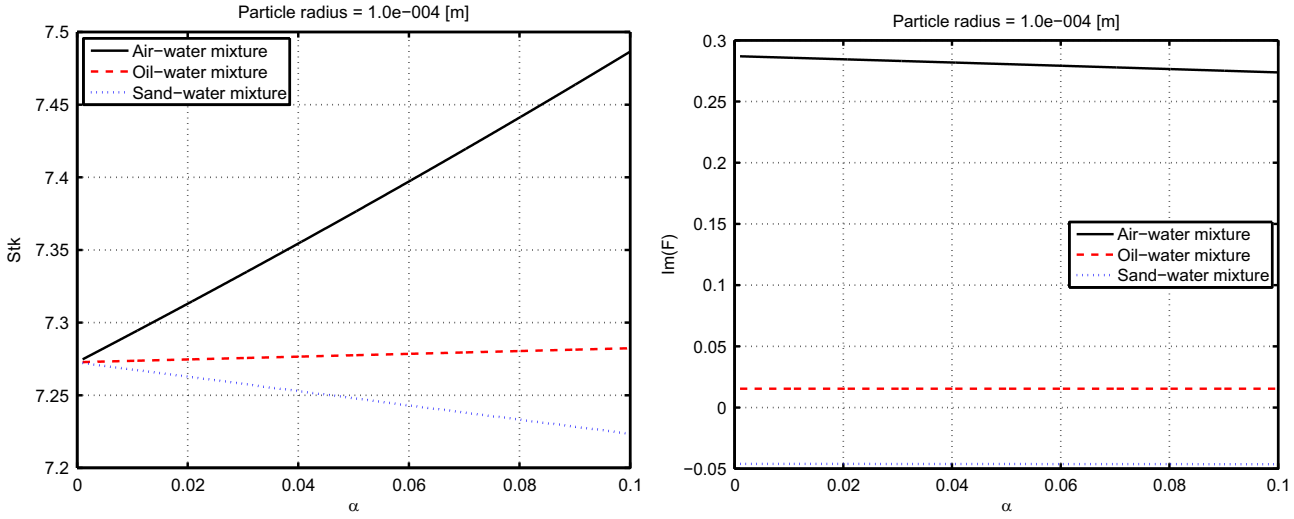

Fig. 9. Fixed particle radius. Left: *Stk* vs. α and right: $Im(F)$ vs. α.

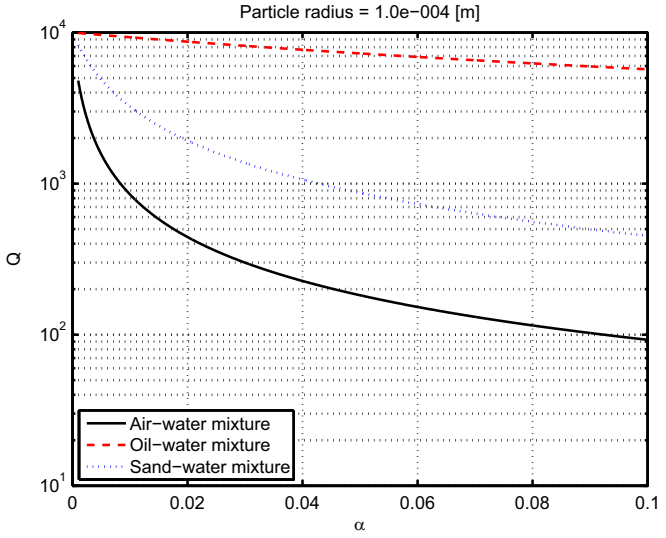

Fig. 10. Fixed particle radius. Q vs. α.

(GVF). The theory is applicable for a GVF below 10%.

8.3.1. Scaling of the quality factor with GVF

In [9], the damping ratio ζ is treated instead of the quality factor:

$$\zeta = \frac{1}{2Q} \tag{62}$$

Using Q_{total} from Eq. (52), we can re-write this as:

$$\zeta = \frac{\frac{c}{\Omega} + (\rho_f - \rho_p)\alpha V_{f-p} Im(F)}{2M_{\text{eff}}} \tag{63}$$

From Eq. (63) we see that the theory implies that ζ increases linearly with α. This agrees with measurements in [9].

8.3.2. Relative motion of fluid and particles

The bubble theory provides detailed information on the relative motion of the fluid and the particles. The starting point is the real and imaginary part of F; this is shown in Fig. 22.

We can use F to calculate B and ϕ defined in Eqs. (39) and (40), see Fig. 23.

The decoupling ratio B is a measure of the amplitude of the particle motion relative to the fluid; a number greater (less) than one means that the particle oscillates with larger (smaller) amplitude than the

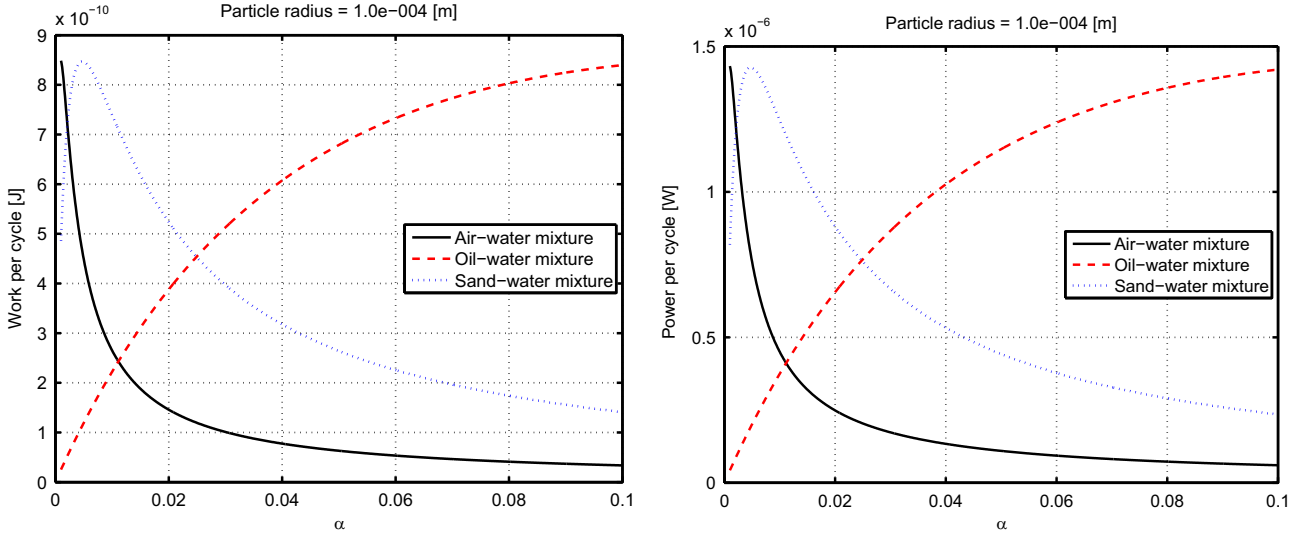

Fig. 11. Fixed particle radius. Left: W_p vs. α and right: P_p vs. α.

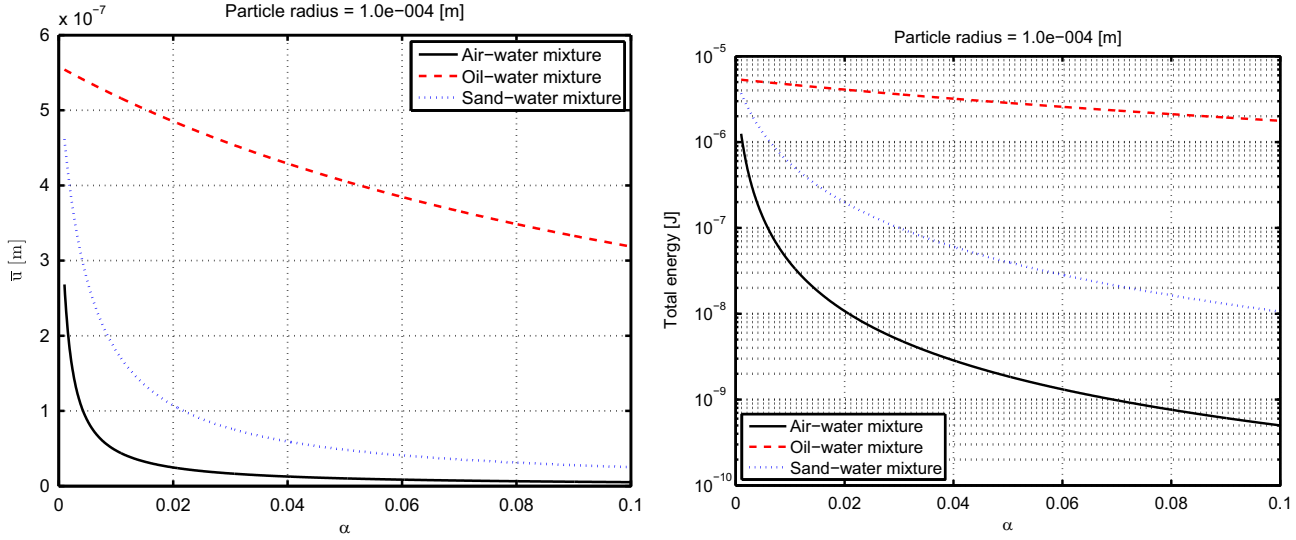

Fig. 12. Fixed particle radius. Left: $\bar{u}$ vs. α and right: E_{total} vs. α.

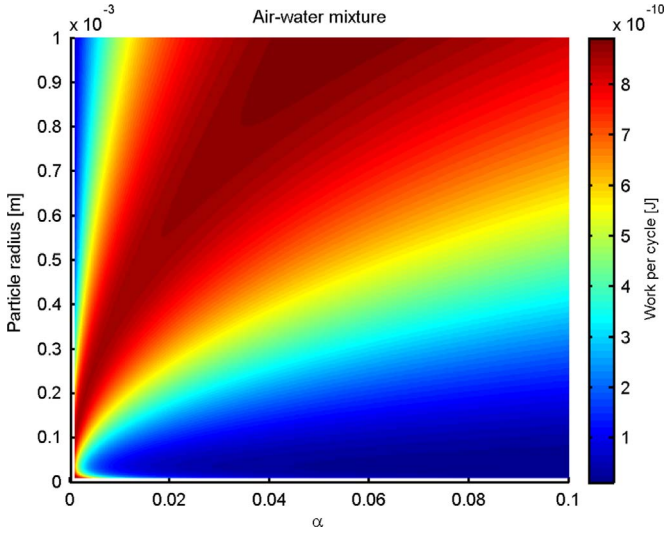

Fig. 13. Air–water mixture: W_p vs. particle radius and α.

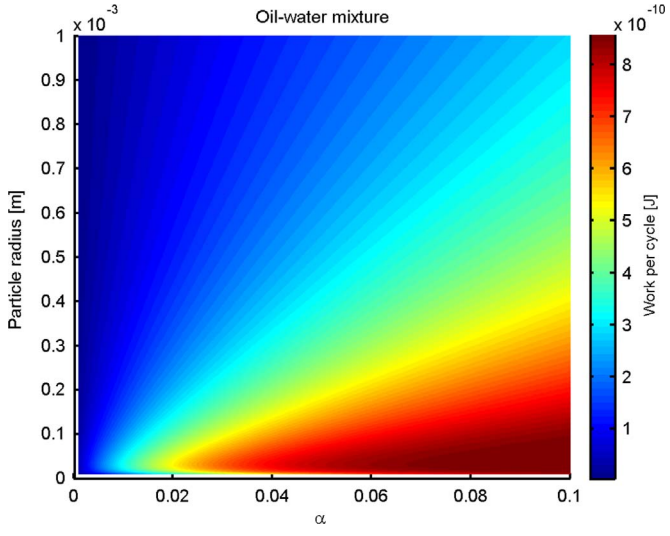

Fig. 15. Oil–water mixture: W_p vs. particle radius and α.

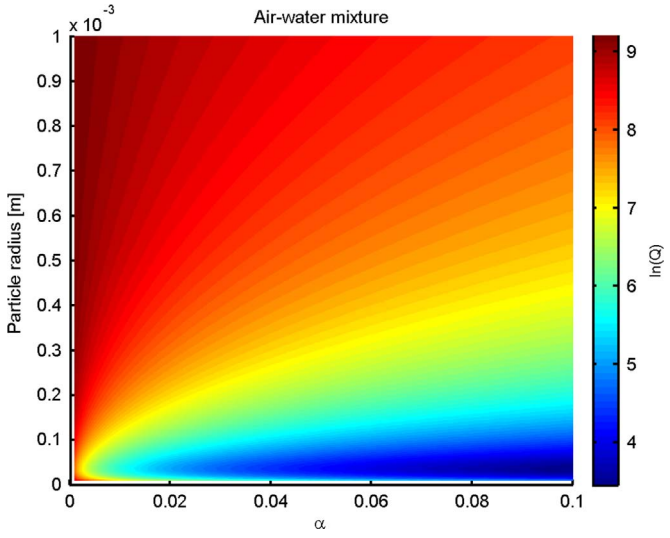

Fig. 14. Air–water mixture: ln (Q) vs. particle radius and α.

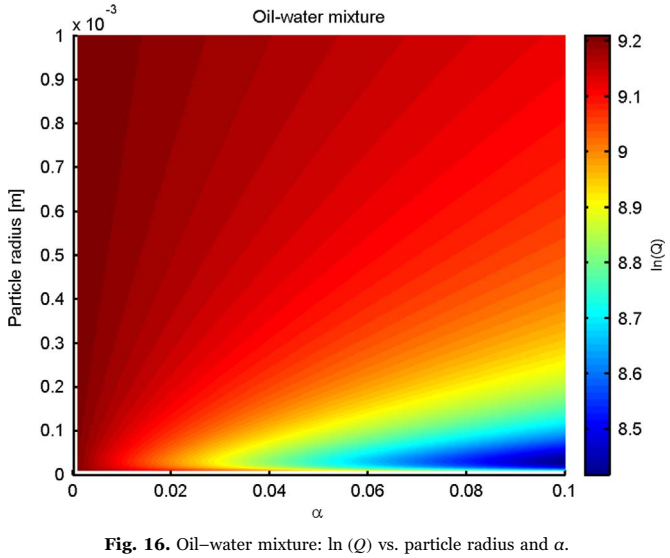

Fig. 16. Oil–water mixture: ln (Q) vs. particle radius and α.

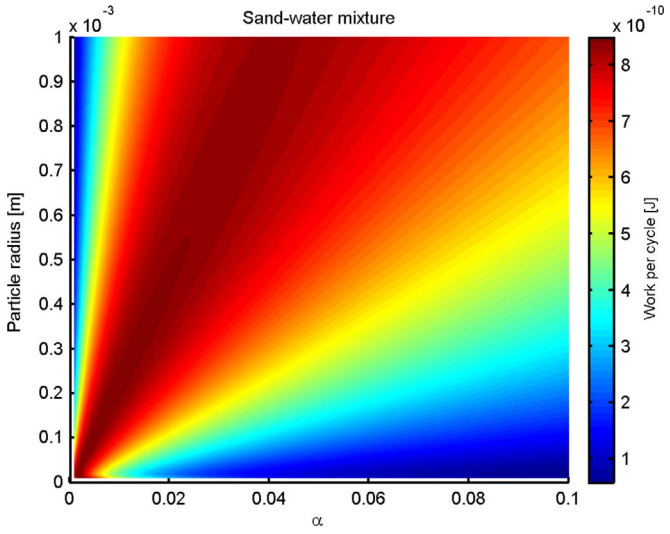

Fig. 17. Sand–water mixture: W_P vs. particle radius and α.

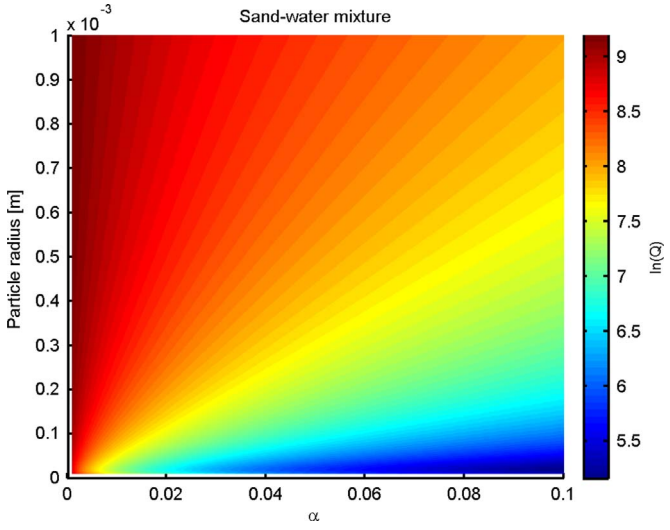

Fig. 18. Sand–water mixture: ln (Q) vs. particle radius and α.

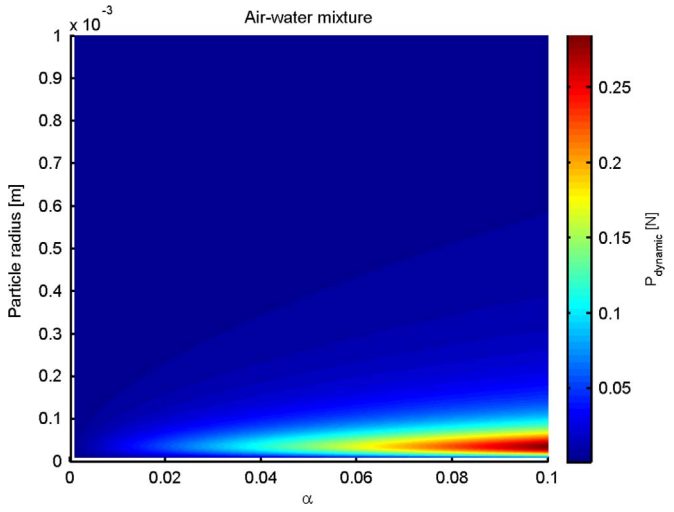

Fig. 20. Air–water mixture: driver force vs. particle radius and α.

Table 1
Material properties at 80 °C. The speed of sound c_s is provided for reference, it is not used.

Material	ρ (kg/m^3)	μ (kg/ms)	c_s (m/s)
Air	1	2.1×10^{-5}	377
Water	972	0.36×10^{-3}	1554

fluid, respectively. For an air–water mixture, the amplitude of the air oscillation will be larger than the amplitude of the water oscillation. In [9], the provided frequency ($\omega_{f-p} = 33.75\ \mathrm{s}^{-1}$) and bubble radius ($a = 1.2$ mm) leads to a *Stk* of about 5; however, B for this value (2.8) is much larger than what is observed in [9] (1.2).

The phase shift ϕ provides information on the relative motion of particles and the fluid: A positive (negative) ϕ means that the particles are leading (lagging) the fluid, respectively. The magnitude of ϕ is a measure of the amount of decoupling. From [9], we estimate ϕ to be roughly 20°. From the theory, we would expect a phase shift of 10°.

Based on these results, we suggest one possible explanation for the discrepancy between theory and measurements. If *Stk* is 1 instead of 5,

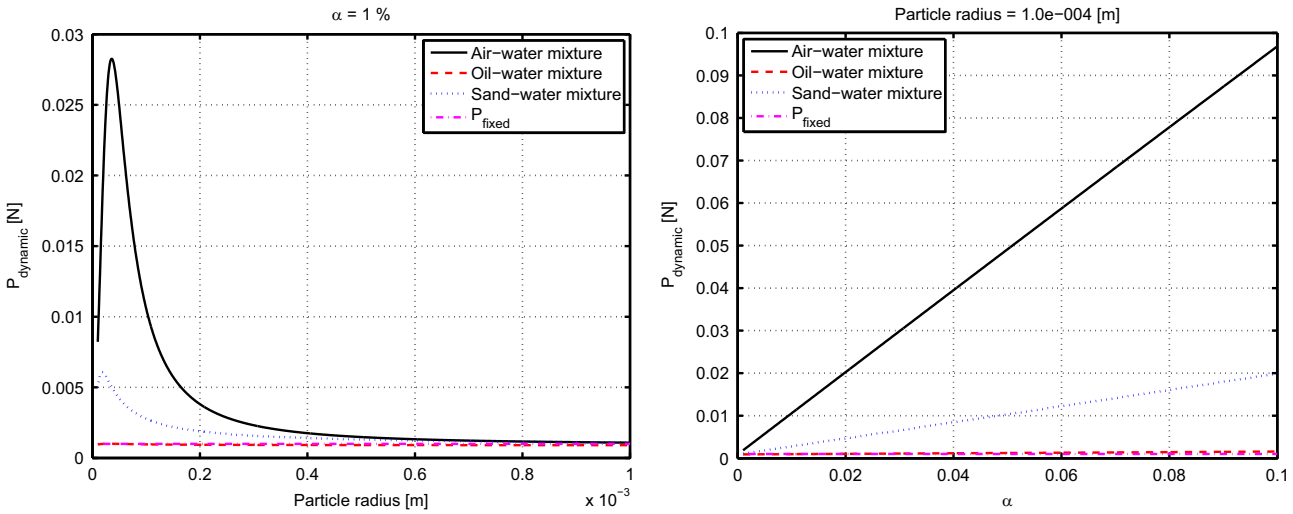

Fig. 19. Driver force for mixtures. Left: fixed α and right: fixed particle radius.

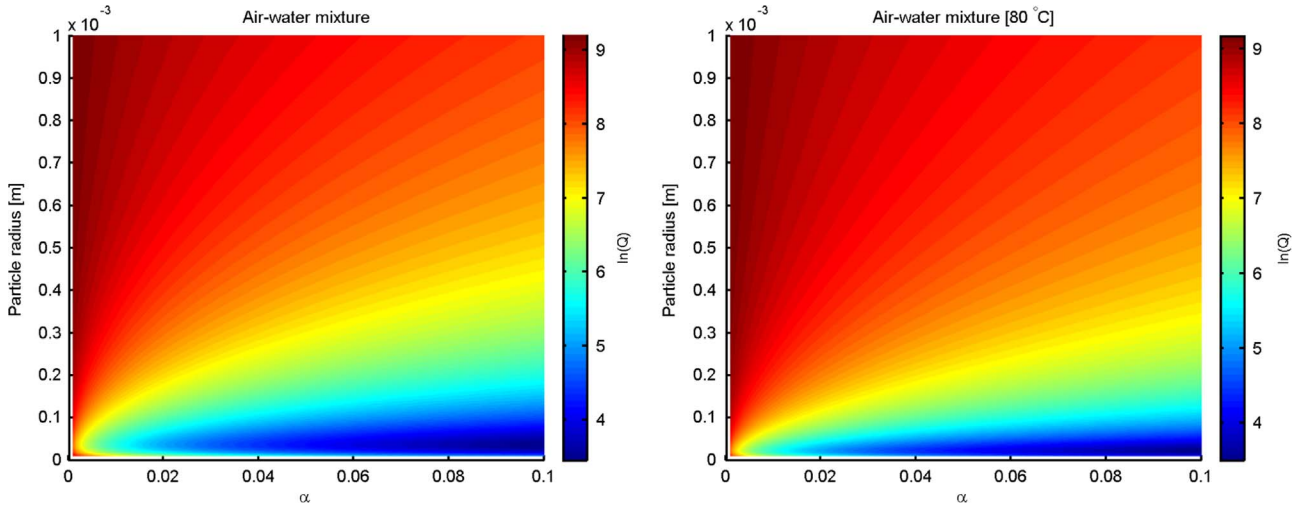

Fig. 21. Air–water mixture: ln (Q) vs. particle radius and α. Left: room temperature and right: 80 °C.

the theory would agree with the measurements. Such a reduction of *Stk* would imply that the bubble radius is five times smaller than stated in [9], i.e. around 0.2 mm.

8.3.3. Flow speed and driver force

The bubble theory assumes that the particles are non-interacting and homogeneously dispersed throughout the fluid. Thus, we expect best agreement with measurements for high flow speed. However, there is no explicit flow speed dependency in the bubble theory. For a GVF below 10%, the measurements do not show a significant dependency on flow speed. This is in line with the theory.

For a GVF below 10%, it is shown in [9] that the damping is independent of the magnitude of the applied force. This can also be seen from Eq. (63) which does not include P.

9. Conclusions

In this paper we have derived the work and power per cycle from damping due to decoupling based on the bubble theory. The expressions can be implemented from this paper combined with the information in [2].

We have presented three examples where water is the continuous phase, while the dispersed phase is air, oil and sand. For the corresponding measurement errors, see [2].

We have included a simple structural model to provide realistic results.

Quality factors are calculated based on two damping contributions: (i) structural damping and (ii) damping due to decoupling.

Two applications of the work are presented: a design guide to calculate the driver force required for varying damping and a comparison of damping due to changes of the mixture and tube temperature. Finally, the bubble theory is compared to measurements: qualitatively, they agree.

Acknowledgements

The author is grateful to Dr. John Hemp for discussions and to a reviewer for referring to [9].

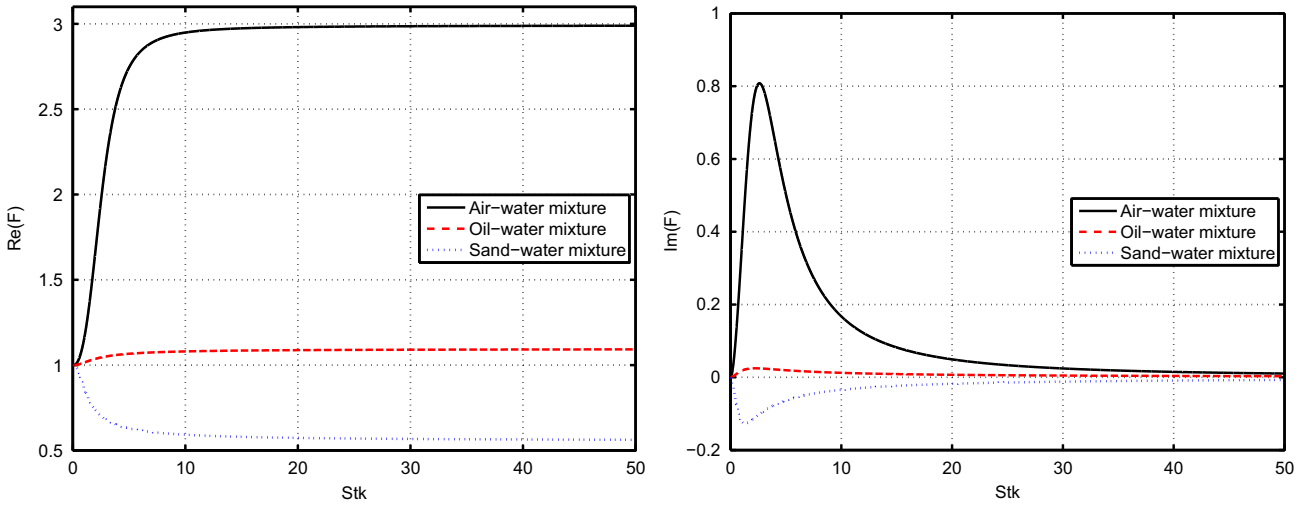

Fig. 22. Left: real part of F and right: imaginary part of F.

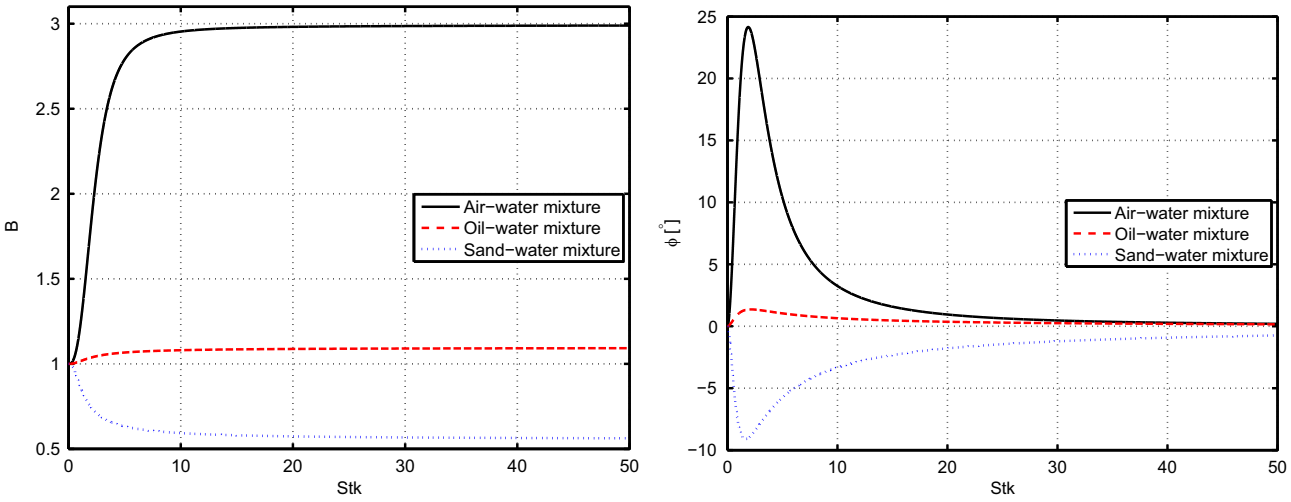

Fig. 23. Left: decoupling ratio B and right: phase shift ϕ.

Appendix A. Heating of mixture

We assume that no heat is transferred from the mixture to other parts of the system, e.g. the tube wall. For very low flow speed, this assumption will no longer hold.

A.1. General formula

The temperature increase of the mixture is:

$$\Delta T_{f-p} = \frac{E_{f-p}}{c_f M_f + c_p M_p}, \tag{A.1}$$

where c_f and c_p are specific heat capacities and E_{f-p} is the total energy being transferred into the mixture during N cycles:

Table A1
Specific heat capacities at room temperature.

Material	Specific heat capacity (J/kg K)
Water	4182
Air	1005
Oil	2000
Sand	700

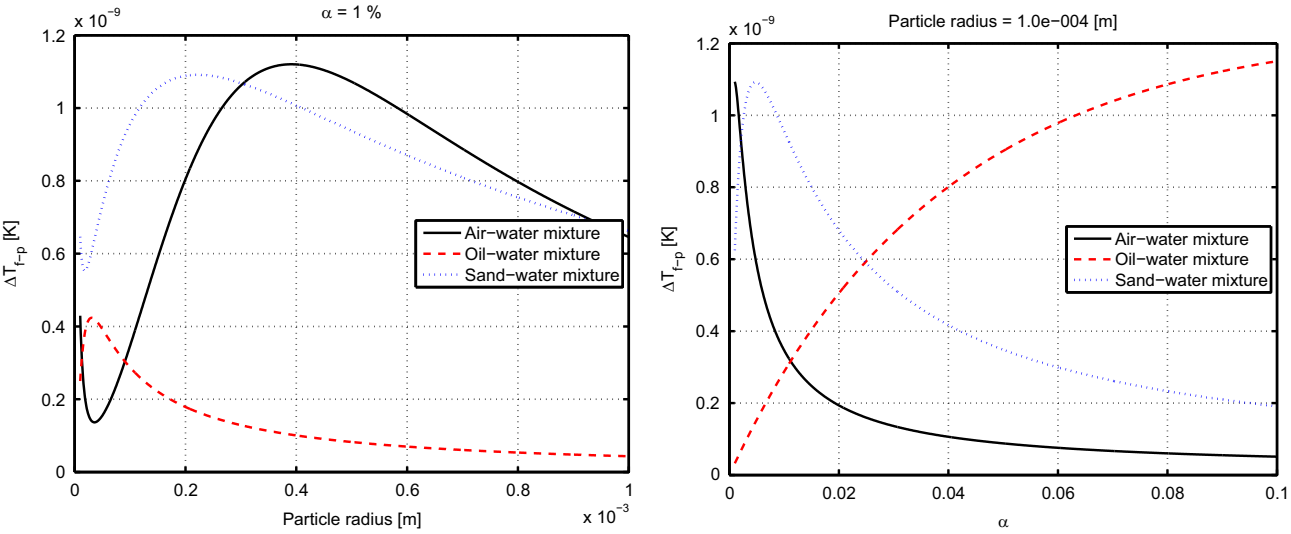

Fig. A1. Temperature increase of mixtures. Left: fixed α and right: fixed particle radius.

$$E_{f-p} = W_p \times N \tag{A.2}$$

The cycle time is:

$$t_c = \frac{2\pi}{\omega_{f-p}} \tag{A.3}$$

We consider a mixture moving with a mean flow speed v_m. The mixture will stay inside the flowmeter for a certain amount of time:

$$\Delta t = \frac{L}{v_m} \tag{A.4}$$

The number of cycles is the total time Δt divided by the cycle time:

$$N = \frac{\Delta t}{t_c} = \frac{L}{v_m} \times \frac{\omega_{f-p}}{2\pi} \tag{A.5}$$

Combining Eqs. (A.1), (A.2) and (A.5) we can write:

$$\Delta T_{f-p} = \frac{W_p L \omega_{f-p}}{2\pi v_m (c_f M_f + c_p M_p)} \tag{A.6}$$

A.2. Examples

We use a mean flow speed v_m=1 m/s.
The specific heat capacities used are in Table A1. Note that the specific heat capacities for oil and sand are approximations.
Results are shown for fixed α and fixed particle radius in Fig. A1. The maximum mixture temperature increase is of the order 10^{-9} K, i.e. minute.

References

[1] J. Hemp, Reaction Force of a Bubble (or droplet) in a Liquid Undergoing Simple Harmonic Motion, 2003, pp. 1–13 (Unpublished).
[2] N.T. Basse, A review of the theory of Coriolis flowmeter measurement errors due to entrained particles, Flow Meas. Instrum. 37 (2014) 107–118.
[3] T. Wang, R. Baker, Coriolis flowmeters: a review of developments over the past 20 years, and an assessment of the state of the art and likely future directions, Flow Meas. Instrum. 40 (2014) 99–123.
[4] J.A. Weinstein, The Motion of Bubbles and Particles in Oscillating Liquids with Applications to Multiphase Flow in Coriolis Meters, University of Colorado, Boulder, Colorado, USA, 2008.
[5] J.M. Gere, B.J. Goodno, Mechanics of Materials, 8th ed., Cengage Learning, Stamford, USA, 2013.
[6] W. Weaver Jr, S.P. Timoshenko, D.H. Young, Vibration Problems in Engineering, 5th ed., John Wiley and Sons, New York, USA, 1990.
[7] J. Kutin, I. Bajsić, Stability-boundary effect in Coriolis meters, Flow Meas. Instrum. 12 (2001) 65–73.
[8] J. Kutin, I. Bajsić, An analytical estimation of the Coriolis meter's characteristics based on modal superposition, Flow Meas. Instrum. 12 (2002) 345–351.
[9] C. Charreton, C. Béguin, A. Ross, S. Étienne, M.J. Pettigrew, Two-phase damping for internal flow: physical mechanism and effect of excitation parameters, J. Fluids Struct. 56 (2015) 56–74.